HHS Public Access

Author manuscript

Bioorg Chem. Author manuscript; available in PMC 2024 July 11.

Published in final edited form as:

Bioorg Chem. 2024 February ; 143: 107103. doi:10.1016/j.bioorg.2024.107103.

Platanosides from *Platanus* × *acerifolia*: New molecules, SAR, and target validation of a strong lead for drug-resistant bacterial infections and the associated sepsis

Xi-Ying Wu[a,b,c,1], **Ze-Yu Zhao**[a,b,1], **Ezzat E.A. Osman**[d], **Xiao-Juan Wang**[e,f], **Yeun-Mun Choo**[g,*], **Menny M. Benjamin**[f], **Juan Xiong**[b], **Mark T. Hamann**[f,*], **Cheng Luo**[h], **Jin-Feng Hu**[a,b,f,*]

[a] Institute of Natural Medicine and Health Products, School of Pharmaceutical Sciences, Zhejiang Provincial Key Laboratory of Plant Evolutionary Ecology and Conservation, Taizhou University, Zhejiang 318000, PR China

[b] School of Pharmacy, Fudan University, Shanghai 201203, PR China

[c] Shanghai Skin Disease Hospital, Tongji University School of Medicine, Shanghai 200443, PR China

[d] Department of Medicinal Chemistry, Theodor Bilharz Research Institute, Kornaish El-Nile St., Giza 12411, Egypt

[e] School of Pharmacy, Lanzhou University, Lanzhou 730000, Gansu, PR China

[f] Colleges of Pharmacy and Medicine, Medical University of South Carolina, Charleston 29425-5700, USA

[g] Chemistry Department, Faculty of Science, University of Malaya, Kuala Lumpur 50603, Malaysia

[h] State Key Laboratory of Drug Research, Shanghai Institute of Materia Medica, Chinese Academy of Science, Shanghai 201203, PR China

Abstract

Three undescribed (**1**–**3**) and nine known (**4**–**12**) platanosides were isolated and characterized from a bioactive extract of the May leaves of *Platanus* × *acerifolia* that initially showed inhibition against *Staphylococcus aureus* Targeted compound mining was guided by an LC-MS/MS-based molecular ion networking (MoIN) strategy combined with conventional isolation procedures from a unique geographic location. The novel structures were mainly determined by 2D NMR and computational (NMR/ECD calculations) methods. Compound **1** is a rare acylated

* Corresponding authors at: Institute of Natural Medicine and Health Products, School of Pharmaceutical Sciences, Zhejiang Provincial Key Laboratory of Plant Evolutionary Ecology and Conservation, Taizhou University, Zhejiang 318000, PR China (J.-F. Hu). ymchoo@um.edu.my (Y.-M. Choo), hamannm@musc.edu (M.T. Hamann), jfhu@fudan.edu.cn, jfhu@tzc.edu.cn, huji@musc.edu (J.-F. Hu).

[1]Xi-Ying Wu and Ze-Yu Zhao contributed to the work equally and should be regarded as co-first authors.

Declaration of competing interest

The authors declare that they have no known competing financial interests or personal relationships that could have appeared to influence the work reported in this paper.

Appendix A. Supplementary data

Supplementary data to this article can be found online at https://doi.org/10.1016/j.bioorg.2024.107103.

kaempferol rhamnoside possessing a truxinate unit. **6** (*Z,E*-platanoside) and **7** (*E,E*-platanoside) were confirmed to have remarkable inhibitory effects against both methicillin-resistant *S. aureus* (MIC: ≤ 16 μg/mL) and glycopeptide-resistant *Enterococcus faecium* (MIC: ≤ 1 μg/mL). These platanosides were subjected to docking analyses against FabI (enoyl-ACP reductase) and PBP1/2 (penicillin binding protein), both of which are pivotal enzymes governing bacterial growth but not found in the human host. The results showed that **6** and **7** displayed superior binding affinities towards FabI and PBP2. Moreover, surface plasmon resonance studies on the interaction of **1**/**7** and FabI revealed that **7** has a higher affinity (K_D = 1.72 μM), which further supports the above *in vitro* data and is thus expected to be a novel anti-antibacterial drug lead.

Keywords

Platanus × *acerifolia*; Platanosides; Molecular ion networking (MoIN); Antibacterial; *Staphylococcus aureus* ; *Enterococcus faecium* ; Structure-activity relationship (SAR); Molecular docking; Target validation

1. Introduction

Sepsis or septicaemia is a life-threatening immune-system response to a bacterial, viral, parasitic, or fungal infection. An estimated 50 million cases of sepsis occur each year, leading to about 11 million deaths globally [1]. Thus, sepsis is considered the leading cause of preventable death in the world by the Global Sepsis Alliance. *Staphylococcus aureus* causes an estimated 50 % of sepsis and is thus a primary concern regarding drug resistance [2]. *S. aureus* toxins lead to tissue necrosis [3] much like acetaminophen (paracetamol, APAP) induced liver toxicity. Both result in an increase in procalcitonin (PCT), which is used as a measure of both bacteria-induced sepsis and liver damage by APAP overdose and is thus recognized as one of the most critical bacterial-causing diseases in humans [4]. The treatment choices for *S. aureus* are usually penicillin and vancomycin. However, serious side effects and drug resistance limit their utility [5,6].

Natural products (NPs) and their derivatives have historically contributed significantly to pharmacotherapy, especially for infectious diseases. When compared to the synthetic classes, NPs demonstrated highly impressive structural diversity and complexity. In fact, since the golden age of antibiotics in the mid-20th century, NPs have always been serving as powerful therapeutics against pathogenic bacteria [7]. For instance, over the time frame from 1981 to 2019, of the 162 approved anti-bacterial agents, 89, or 54.9 %, are NPs or their structural analogues [8]. However, new classes of antibiotics have been rare, and the lack of research and resources have resulted in a two-decade-long antibiotic development void [9]. Thus, the significance of this new class could not be greater.

Identifying new molecules early in the workflow using Molecular Ion Network (MoIN) minimizes time, effort, and the cost of large screening campaigns [10,11]. The visualization of networks using Cytoscape enables the direct observation of similarities and differences between two or more samples in which similar entities within the network are clustered together. In contrast, disparate or unique entities are grouped separately. With the use of this

approach, platanosides (PTSs), as well as their analogs, were found in the early workflow of purification [12].

PTSs belong to a unique class of flavonoids, which generally consist of the components of the kaempferol flavone rhamnose glycoside moiety with *p*-coumaroyl group(s) attached to the carbohydrate unit. The leaves of the Oriental plane tree (*P. orientalis*, chinar) and American sycamore (*P. occidentalis*, American plane tree) have been documented to be rich sources of flavonoids (incl. PTSs) with interesting antibacterial activity against methicillin-resistant *S. aureus* (MRSA) [13–19]. Such flavonoids were often encountered from the buds [20–28] of *Platanus* × *acerifolia* Willd (P*a*W), but only a few have been previously reported from its leaves [29,30]. Most recently, PTSs possessing significant *S. aureus* inhibitory activities have been unveiled from the January (Winter) P*a*W leaves [31].

In this study, the EtOAc-soluble fraction of the 90 % MeOH extract of the P*a*W leaves collected in the Spring (May 2017) showed antibacterial activity against *S. aureus*. Subsequently, an in-depth investigation of this fraction was carried out using various chromatographic techniques due to its strong potential to inhibit bacterial growth of *S. aureus*, resulting in the isolation and characterization of three undescribed flavonol glycosides (**1**–**3**) and nine known acylated kaempferol rhamnosides (**4**–**12**) (Figs. 1, 2). Furthermore, the antibacterial activities against both MRSA and glycopeptide-resistant *Enterococcus faecium* (GREfm) of the isolates were evaluated, showing the MICs of **6** (*Z, E*-platanoside) and **7** (*E, E*-platanoside) were 4–16 μg/mL (MRSA) and 0.5–1 μg/mL (GREfm).

2. Results and discussion

2.1. Isolation and structural elucidation

Isolation of the unreported molecules was facilitated under the guidance of UPLC-HRMS/MS (positive mode)-based molecular ion networking (MoIN) as enabled through the Cytoscape platform (https://cytoscape.org). This analysis revealed three unique signals at *m*/*z* 765.2, 595.1, and 579.2 with different retention times (Fig. 1). Subsequently, target purification of these *m*/*z* 579, 595, 765 metabolites afforded compounds **1**, **2**, and **3**.

Compound **1** was obtained as a yellow amorphous powder, and its molecular formula was established as $C_{39}H_{34}O_{15}$ based on the protonated molecule at *m*/*z* 743.1975 $[M + H]^+$ detected by HRESIMS (calcd. 743.1970) and ^{13}C NMR data (Table S1). The UV spectrum (Fig. S1) exhibited two characteristic absorptions at 269 and 340 nm, indicating the presence of a 3-OH substituted flavanol skeleton [32,33], which was corroborated by the absorption bands at 3412 (br, hydroxy), 1718 (ester carbonyl), 1654 (conjugated carbonyl), and 1515 (aromatic ring) cm^{-1} in its IR spectrum (Fig. S2) [34]. The ^1H NMR spectrum (Table S1) revealed an AA′BB′ spin system due to the aromatic proton signals at δ_H 7.82 (2H, br d, J = 8.3 Hz, H-2′, H-6′) and 6.97 (2H, br d, J = 8.3 Hz, H-3′, H-5′), along with two meta-coupled doublets at δ_H 6.47 (1H, br s, H-8) and 6.27 (1H, br s, H-6), as well as three hydroxyl groups at δ_H 12.63 (1H, s), 11.02 (1H, s), and 10.32 (1H, s), characteristic resonance for 5-OH, 7-OH, and 4′-OH, respectively. Undoubtedly, the data above delineated a kaempferol backbone [35]. Meanwhile, the ^1H–^1H COSY motif (Fig. 3) of H-6″/H-5″/

H-4″/H-3″/H-2″/H-1″ in conjunction with the ^{13}C (Table S1) and HSQC NMR analysis (Fig. S5) revealed the existence of an α-rhamnose moiety [13,35], which was found to locate at C-3 due to the key HMBC correlation from H-1″ (δ_H 5.38) to C-3 (δ_C 135.07) (Fig. 3). Besides, four methine protons at δ_H 4.03 (1H, dd, J = 9.8, 6.0 Hz, H-7a), 4.17 (1H, dd, J = 9.8, 8.8 Hz, H-7b), 3.72 (1H, dd, J = 9.5, 6.0 Hz, H-8a), 3.89 (1H, dd, J = 9.5, 8.8 Hz, H-8b) were observed and the correlations of H-7a/H-7b/H-8b/H-8a/H-7a in ^{1}H–^{1}H COSY experiment (Fig. 3) confirmed the presence of a cyclobutane ring [34]. In addition, two 4-hydroxyphenyl groups were constructed owing to the observation of two sets of well-resolved proton signals: δ_H 6.83 (2H, br d, J = 8.0 Hz, H-2a, H-6a), 6.87 (2H, br d, J = 7.8 Hz, H-2b, H-6b), 6.52 (2H, br d, J = 8.0 Hz, H-3a, H-5a) and 6.54 (2H, br d, J = 7.8 Hz, H-3b, H-5b), together with δ_H 9.15 (1H, s) for 4a-OH and 9.17 (1H, s) for 4b-OH. The HMBC correlations (Fig. 3) from H-2a/6a to C-7a (δ_C 44.80), H-2b/6b to C-7b (δ_C 45.18), H-7a to C-9a (δ_C 173.53), and H-7b to C-9b (δ_C 175.24) suggested that the attachment of the two 4-hydroxyphenyl groups as vicinal arrangement in the truxinyl (head-to-head). Furthermore, the HMBC correlation between H-3″ (δ_H 5.03) and C-9a (δ_C 173.53) indicated the attachment of truxinate unit at C-3″ of L-rhamnose.

The relative configuration of the cyclobutane ring was determined via the NOESY analysis (Fig. 3). The NOE correlations of H-7a/H-7b, H-8a/H-8b, H-8a/H-2a (H-6a), and H-8b/H-2b (H-6b) established *cis*-configurations between H-7a and H-7b, as well as between H-8a and H-8b, but a *trans*-geometry between H-7a and H-8a, which is typically conserved in a β-truxinate structure. In fact, the NMR data of the cyclobutane protons (Table S1) were in good agreement with those of biginkgoside A, a β-truxinic-type flavonol glycoside cyclodimers isolated from *Ginkgo biloba* leaves in our group [34]. Accordingly, the most probable stereoisomer is either (7a*R**,7b*S**,8a*S**,8b*R**)-**1**A or (7a*S**,7b*R**,8a*R**,8b*S**)-**1**B. In order to finalize the relative configuration of **1**, the ^{13}C NMR calculations for both **1**A and **1**B were performed by means of GIAO at the mPW1PW91/6–31 g (d, p) level [36,37]. The results obtained through DP4 + probability analyses predicted **1**A to match well with the experimental data of **1** with 100.00 % probability (Fig. 4, Tables S2 and S3). The absolute configuration of **1** was then established by comparing the experimental and calculated electronic circular dichroism (ECD) spectra of **1**A. The negative Cotton effects (CEs) around 227 nm and 318 nm, along with the positive CE at 252 nm in the experimental ECD spectrum, are congruent with those in the calculated one but antipodal to the isomer [(7a*S*,7b*R*,8a*R*,8b*S*)- **1**] (Fig. 5, Table S4). Thus, the structure of compound **1** was finally ascertained as (7a*R*,7b*S*,8a*S*,8b*R*)-kaempferol-3-*O*-α-L-(3″-β-truxinate)-rhamnopyranoside. Naturally occurring compounds possessing a truxinate unit have been discussed in a preceding work [34]. The plausible biosythetic ptathway of **1** was most likely derived from a precursor (i.e., **8**) and a *p*-coumaric acid via a [2 + 2]-cycloaddition reaction [34].

Compound **2** was isolated as a pale yellow powder, and its positive-mode HRESIMS data showed a sodium adduct ion at m/z 601.1322 $[M + Na]^+$ (calcd. 601.1316), which in conjunction with ^{13}C NMR data (Table S5) corresponded to the molecular formula $C_{30}H_{26}O_{12}$. The absorption bands at 253 and 313 nm in the UV spectrum, and 3442 (hydroxy), 1655 (conjugated carbonyl), and 1511 (aromatic ring) cm^{-1} in the IR spectrum were characteristic for a flavonol structure [34]. A comparison of the NMR data of **2** (Table

S5) with those of **1** (Table S1) displayed close structural similarity. Unlike compound **1**, the typical signals of the *β*-truxinate group attached at C-3″ were absent in **2**. Instead, the presence of a (*Z*)-*p*-coumaroyl moiety was evidenced from the ^{1}H NMR data [δ_H 7.80 (2H, br d, *J* = 8.4 Hz, H-2′″, 6′″), 6.93 (1H, d, *J* = 12.8 Hz, H-7′″), 6.82 (2H, br d, *J* = 8.4 Hz, H-3′″, 5′″), and 5.93 (1H, d, *J* = 12.8 Hz, H-8′″)], the correlations between H-7′″/H-8′″, H-3′″/H-2′″ and H-6′″/H-5′″ in ^{1}H–^{1}H COSY spectrum and the HMBC correlations from H-7′″ to C-2′″ (6′″) (δ_C 134.83) and from H-8′″ to C-1′″ (δ_C 128.51) of *p*-coumaroyl moiety. Furthermore, the coumaroyl was assigned to the 3″-position of the 3-*O*-rhamnosyl moiety since the rhamnosyl H-3″ signal was shifted downfield to δ_H 5.12 (1H, br d, *J* = 10.1 Hz) and C-3″ downfield at δ_C 75.74. According to all the NMR data, including the obvious HMBC correlations (Fig. S15), compound **2** showed great resemblance to another compound previously isolated from the buds of *P. orientalis*, known as kaempferol 3-*O*-*α*-L-(3″-*E*-*p*-coumaroyl)-rhamnopyranoside [27]. Therefore, compound **2** was determined as kaempferol 3-*O*-*α*-L-(3″-*Z*-*p*-coumaroyl)-rhamnopyranoside.

Compound **3** was obtained as a yellow powder. The molecular formula was recorded to be $C_{30}H_{26}O_{13}$ from the molecular ion peak $[M + Na]^+$ at *m*/*z* 617.1273 (calcd. 617.1266) in the positive-mode HRESIMS data, which was in accordance with ^{13}C NMR data (Table S5). The UV (λ_{max} 269, 315 nm) and IR (ν_{max} 3442, 1655, 1510 cm^{-1}) spectra were alike to that of compound **2**, corresponding to a flavonol structure. The NMR spectra of compounds **3** and **2** were also similar (Table S5), though a main difference resided in an additional hydroxyl group of B-ring in **3**. Specifically, a 1,3,4-trisubstituted aromatic ring at δ_H 7.40 (1H, br s, H-2′), 7.37 (1H, br d, *J* = 8.3 Hz, H-6′), and 6.97 (1H, d, *J* = 8.3 Hz, H-5′) indicated the presence of a 3′,4′-dihydroxy B ring system in quercetin aglycone [38]. Another two differences were observed when comparing the ^{1}H NMR data of compounds **3** and **2**: H-2″ was shifted downfield (Δ + 1.10 ppm), while H-3″ was shifted upfield (Δ − 1.14 ppm) in **3**, indicating that the (*Z*)-coumaroyl moiety was located at C-2″ position. Likewise, compound **3** structurally bears a close resemblance to 2″-(*E*)-*p*-coumaroyl quercitrin with the only exception for the configuration of *p*-coumaroyl at C-2″ position [39]. Thus, **3** was identified as quercetin-3-*O*-*α*-L-(2″-*Z*-*p*-coumaroyl)-rhamnopyranoside.

2.2. Antibacterial activity of isolated compounds

Inspired by the fact that flavonoids are effective resources for designing antimicrobial drugs and the results of the preliminary antibacterial bioassay, the isolates **1**–**12** were initially evaluated for their inhibition effects against Newman *S. aureus*, with vancomycin-HCl (Van. HCl) was used as a positive control. The results (Table S6) demonstrated compounds **6** and **7** as active ingredients with MIC values of 4–8 μg/mL. As shown in Table 1, 6 exhibited a greater potent inhibitory effect against MRSA (MIC: 4 μg/mL) than the positive control (MIC: 8 μg/mL). Besides, both **6** and **7** significantly inhibited the growth of GREfm with MIC values of 0.5 and 1 μg/mL, respectively. The structure–activity relationship (SAR) of the related compounds showed that the flavonoid moiety connected to the *p*-coumaroyl group through the sugar and the hydroxy groups at the positions of C-5, C-7, and C-4′ were vital for the antibacterial activity, which is consistent with the previous reports [13,31]. Additionally, the configuration around the double bonds of the *p*-coumaroyl group plays a

decisive role. Specifically, the *Z*-configuration of the *p*-coumaroyl unit in the R_2-position showed enhanced activity compared with the *E*-configuration and vice versa for R_3-position.

2.3. In-silico molecular docking study

In this context, the compounds derived from the present study were subjected to docking analyses against FabI (enoyl-ACP reductase) and PBP1/2 (penicillin binding protein), both of which are pivotal enzymes governing bacterial growth. Importantly, neither of these enzymes exhibit a substantial degree of conservation in the human host [40,41]. As a result, these enzymes could function as viable anti-bacterial targets, with a high likelihood of compounds effectively targeting these enzymes across various species.

FabI serves as a catalyst in the biosynthesis of fatty acids, essential components within the bacterial cell wall structure. The inhibition of FabI's activity leads to the impediment of bacterial growth [42]. Conversely, PBPs are integral to the synthesis of peptidoglycan, a principal constituent of the bacterial cell wall. PBPs bind to β-lactam antibiotics, such as penicillin, thereby disabling their capacity to synthesize peptidoglycan. Mutations and the amplification of PBPs are orchestrated as defensive mechanisms by bacteria to mitigate the inhibitory effects exerted by β-lactam antibiotics [43,44]. Notably, mutations in the penicillin binding site of PBPs reduce their binding affinity to penicillin, leading to antibacterial resistance. This phenomenon, however, can be circumvented through the use of non-β-lactam antibacterial compounds that bind either to the penicillin binding site or an allosteric binding site. Such compounds have the potential to counteract the resistance mechanism. In essence, investigating the interaction of the studied compounds with FabI and PBPs sheds light on their prospective antibacterial activities.

The molecular docking outcomes exhibited a consistent pattern, wherein larger molecules demonstrated notably improved results. For instance, both di- and mono-coumaroyl derivatives prominently displayed superior binding affinities towards bacterial FabI enzymes (*S. aureus*, *A. baumannii*, and *P. aureginosa*) (Fig. 6), featuring a binding affinity spectrum ranging from −9.1 to −12.3 kcal/mol. Furthermore, this compound set also exhibited robust binding affinities to PBP enzymes, encompassing both the penicillin and allosteric binding sites. Equally noteworthy, the novel compounds **1**–**3** demonstrated impressive binding affinities towards FabI (−9.7 to −11.4 kcal/mol) (Fig. 6) and PBP2 (−8.6 to −9.5 kcal/mol). These outcomes suggest the dual potential of the new compounds as antibacterial agents, thereby regulating bacterial growth.

Although compounds **6** (*Z,E*-platanoside) and **7** (*E,E*-platanoside) both displayed strong binding affinities to the FabI and PBP enzymes of *S. aureus*, a discernible difference emerged. **6** (FabI: −11 kcal/mol; PBP2: −9.2 kcal/mol; PBP2 allosteric site: −9.9 kcal/mol) demonstrated superior affinity compared to compound **7** (FabI: −10.6 kcal/mol; PBP2: −7.1 kcal/mol; PBP2 allosteric site: −9.3 kcal/mol) (Fig. 7). This observation corresponded with the established activity trend for **6** and **7** in the antimicrobial assay (Table 1). Furthermore, despite **1** demonstrating a higher *in-silico* binding affinity compared to **7**, the binding position of **7** resides deeper within the binding pocket. Conversely, **1** binds near the opening of the binding pocket, suggesting a greater likelihood of easier dissociation for **1** as opposed to **7**. Subsequently, surface plasmon resonance (SPR, an essential technique for

hit validation) [45–47] studies on the interaction of the selected platanosides (e.g., **1** and **7**, both samples are available) and FabI (a pivotal enzyme governing bacterial growth) revealed **7** has a higher affinity (K_D = 1.72 μM) than that of **1** (K_D = 5.38 μM) (Fig. 8), aligning with the inhibitory activity observed in antibacterial assays.

A pronounced theme illuminated by the docking outcomes underscores the compelling efficacy of the larger di- and mono-coumaroyl derivatives. These sizable compounds exhibited notable binding affinities across a diverse array of enzymes such as bacterial FabI and PBP1/2. For instance, the molecular docking results demonstrated that larger compounds like **6** and **7** displayed notably strong binding affinities to these enzymes despite marked variations in dimensions and amino acid residues within the binding domains (Table S7).

A comprehensive examination of the binding orientation of the di-coumaroyl compound, exemplified by **6** (*Z,E*-platanoside), to these enzymes, unveiled that the compound's structural scaffold possessed favorable attributes that facilitated its fitting into the binding domains (Fig. 9). Compound **6**, characterized by di-coumaroyl structure, comprised a highly flexible configuration encompassing a flavonol, a glycoside, and two coumaroyl moieties coupled with multiple aromatic rings, carbonyl, and hydroxyl functionalities. The outcomes indicated that the linkages among these structural components are rotatable, while the two coumaroyl appendages can be adjusted and folded accordingly to conform to the binding domains of diverse enzymes. The carbonyl and hydroxyl functionalities demonstrated a propensity to establish multiple hydrogen bonding interactions with specific amino acid residues, whereas the aromatic rings in the flavonol and coumaroyl initiated **π**-**π**, **π**-**σ**, **π**-alkyl, and **π**-sulfur interactions, effectively anchoring **6** within the binding domains.

In summary, the molecular docking analysis revealed that larger compounds, particularly di- and mono-coumaroyl derivatives, including the novel compounds **1**–**3**, exhibited robust binding affinities towards the anti-inflammation and antibacterial targets. The observed binding affinities, along with their consistent correspondence to the experimental antimicrobial activity of compounds **6** (*Z,E*-platanoside) and **7** (*E,E*-platanoside), emphasize the promising potential of these compounds in addressing the intricate interplay between inflammation and bacterial infections.

3. Conclusions

In conclusion, the current investigation confirmed how plants belonging to the *Platanus* genus represent a reliable source of flavonoids to study the SAR and supply the platanosides. Herein, we only conducted the studies on P*a*W leaves. Given the favored antimicrobial activity, the EtOAc-soluble fraction of the 90 % MeOH extract of Spring P*a*W leaves was submitted for further isolation. As a result, three previously undescribed flavonol glycosides (**1**–**3**) were obtained. Interestingly, compound **1** is a rare naturally occurring flavonol glycoside possessing a *β*-truxinate motif [33]. Furthermore, platanosides **6** and **7** exhibited potent inhibitory effects against both MRSA and GREfm. Additional studies are warranted to clarify their antibacterial mechanisms, as well as the possibility of exploring the use of these platanosides in infectious diseases. The effectiveness of the

platanosides against drug-resistant bacteria and organ damage to chemical insults from acetaminophen, a common cause of liver damage leading to liver transplant, makes these molecules a highly promising set of drug leads for the control of sepsis. The in-silico molecular docking results provide compelling evidence supporting the antibacterial potential of the compounds isolated in this study, including the novel compounds **1**–**3**. The alignment between the demonstrated binding affinities and the established antimicrobial efficacy, as observed in platanosides **6** and **7**, underscores the considerable promise embedded within these compounds, effectively poised to navigate the intricate interplay linking inflammation and bacterial infections.

4. Experimental

4.1. General experimental procedures

The optical rotations were measured using an Autopol IV automatic polarimeter. UV absorptions and IR spectra were recorded on a Hitachi U-2900E double beam spectrophotometer and a Thermo Scientific Nicolet Is5 FTIR spectrometer, respectively. NMR spectra were recorded by a Bruker Avance III 400, a Bruker Avance DRX-500, and/or a Bruker Avance 600 MHz spectrometer. Chemical shifts were expressed in δ (ppm) and referenced to the residual solvent signals. ESIMS were measured on a Waters UPLC H-Class-SQD or an Agilent 1100 series mass spectrometer. HRESIMS were recorded on a Bruker Daltonics micro TOF-QII or an AB 5600 + Q TOF spectrometer. Semi-preparative HPLC was performed on a Waters e2695 system with a Waters 2998 PDA and a Waters 2424 ELSD; ODS column (SunFire, 5 μm, 150 × 4.6 mm; SunFire, 5 μm, 250 × 10 mm; Cosmosil, 5 μm, 250 × 10 mm). Flash chromatography was performed on an EZ-L100-P200 (Lisure Science Ltd., Suzhou, China). Column chromatography (CC) was performed using silica gel (100–200 mesh, Kang-Bi-Nuo Silysia Chemical Ltd., Yantai, China), MCI (CHP20P, 75–150 μm, Mitsubishi Chemical Industries, Tokyo, Japan), and Sephadex LH-20 (GE Healthcare Bio-Sciences AB, Uppsala, Sweden). Silica gel-precoated plates (HSGF254, Kang-Bi-Nuo Silysia Chemical Ltd., Yantai, China) were used for TLC detection. Spots were visualized using UV light (254 and/or 365 nm) and by spraying with 10 % H_2SO_4-EtOH.

4.2. Plant materials

The leaves of PaW were collected from Zhangjiang area, Shanghai, China in May 2017 (spring). The plant samples were authenticated by Prof. Ze-Xin Jin (Taizhou University). The voucher specimens [Nos. 20170501, 20171001 (green leaves), 20171002 (fallen leaves) and 20180101] were conserved at the Herbarium of the School of Pharmaceutical Sciences, Taizhou University, China.

4.3. Bacterial strains

Newman Staphylococcus aureus, a methicillin-sensitive strain, and Mu50, a Healthcare-associated methicillin-resistant S. aureus (MRSA) strain isolated in Japan, as well as Van (B), a van-B phenotype glycopeptide-resistant Enterococcus faecium (GREfm) strain isolated in China were kindly supplied by Prof. Lefu Lan (Shanghai Institute of Materia Medica, Chinese Academy of Sciences, Shanghai, China).

4.4. Isolation and purification

The air-dried May leaves were grinded using an electric mill. 35 kg of dry powder were extracted four times using 105 L of 90 % MeOH. The obtained 90 % MeOH extract (5.6 kg) was then suspended in water and extracted with petroleum ether (PE), ethyl acetate (EtOAc) and normal butanol (*n*-BuOH), successively. All the fractions were concentrated by rotatory evaporator till dryness yielding PE (700 g), EtOAc (150 g), and *n*-BuOH (400 g) extracts, which were kept at room temperature for the phytochemical analysis.

The EtOAc fraction (150 g) was loaded to column chromatography over silica gel with a gradient-elution system of EtOAc/MeOH (neat EtOAc → 97.5:2.5 → 95:5 → 90:10 → 80:20, v/v) to yield five main fractions (Fr. 1–Fr. 5). Fr. 1 (22 g) was fractionated by an MCI column (from 30 % MeOH in H_2O to 100 % MeOH) to afford five sub-fractions Fr. 1A–Fr. 1D. Fr. 1B (6 g) was then successively purified using MCI column chromatography (CC) with gradient mobile phase of MeOH/H_2O (from 30 % to 100 %, v/v), Sephadex LH-20 CC, and semi-preparative HPLC [SunFire; flow rate, 3.0 mL/min]. Afterwards, compound **3** (2.2 mg, t_R = 27.5 min) was obtained using semi-preparative HPLC [MeCN/H_2O (containing 0.05 % TFA, v/v) 35:65, v/v], while compounds **1** (20.0 mg, t_R = 18.7 min), **2** (2.3 mg, t_R = 16.5 min), and **11** (22.5 mg, t_R = 14.7 min) were generated by semi-preparative HPLC [MeOH/H_2O (containing 0.05 % TFA, v/v) 60:40, v/v]. Fr. 1C (1 g) was loaded over Sephadex LH-20 CC with MeOH as eluent, and further separated by semi-preparative HPLC [SunFire, MeOH/H_2O (containing 0.05 % TFA, v/v) 60:40, v/v] to give **12** (12.0 mg, t_R = 14.3 min). In a similar way, compounds **4** (35.2 mg, t_R = 24.5 min), **5** (4.1 mg, t_R = 27.1 min), **6** (25.6 mg, t_R = 25.7 min) and **7** (90.3 mg, t_R = 28.9 min) were finally purified by semi-preparative HPLC [1.5 g, MeOH/H_2O (containing 0.05 % TFA, v/v) 70:30, v/v] from Fr. 1D (1.5 g) while compounds **8** (13.6 mg, t_R = 21.8 min), **9** (6.7 mg, t_R = 19.1 min), and **10** (2.9 mg, t_R = 20.5 min) ere garnered from Fr. 2 (2 g) under the same HPLC condition.

4.4.1. Kaempferol- 3-O-α-L-(3″-β-truxinate)-rhamnopyranoside (1)—Yellow amorphous powder; $[\alpha]_D^{20}$ – 133 (*c* 0.1, MeOH); UV (MeOH) λ_{max} (log ε) 271 (3.02), 341 (3.75) nm; ECD (*c* 1.37 × 10^{-3} M, MeCN) λmax (Δ *ε*) 227 (−9.7), 252 (+5.16), 301 (−4.22) nm; IR (film) νmax 3500, 1732, 1655, 1620, 1510, 1385, 1177, 1142, and 1082 cm^{-1}; ^1H NMR and ^{13}C NMR data (in DMSO−d_6), see Table S1; HR-ESIMS *m*/*z* 743.1975 $[M + H]^+$ (calcd. for $C_{39}H_{34}O_{15}$, 743.1970, Δ = 0.6 ppm).

4.4.2. Kaempferol-3-O-α-L-(3″-Z-p-coumaroyl)-rhamnopyranside (2)—Pale yellow powder; $[\alpha]_D^{20}$ – 39 (*c* 0.1, MeOH); UV (MeOH) λ_{max} (log ε) 253 (2.88), 313 (3.92) nm; IR (film) ν_{max} 3442, 2925, 1682, 1655, 1615, 1511, 1382, and 1052 cm^{-1}; ^1H NMR and ^{13}C NMR data (in CD_3OD), see Table S5; HR-ESIMS *m*/*z* 601.1322 $[M + Na]^+$ (calcd. for C30H26O12, 601.1316, Δ = 0.9 ppm).

4.4.3. Quercetin-3-O-α-L-(2″-Z-p-coumaroyl)-rhamnopyranside (3)—Yellow powder; $[\alpha]_D^{20}$ + 9 (*c* 0.1, MeOH); UV (MeOH) λ_{max} (log ε) 269 (2.95), 315 (3.88) nm; IR (film) ν_{max} 3442, 2925, 2850, 1677, 1655, 1615,1510, 1382, and 1045 cm^{-1}; ^1H NMR and ^{13}C NMR data (in CD_3OD), see Table S5; HR-ESIMS *m*/*z* 617.1273 $[M + Na]^+$ (calcd. for C30H26O13, 617.1266, Δ = 1.1 ppm).

4.5. Computational calculations of ^{13}C NMR and ECD data

The procedures of NMR/ECD calculations referred to the preceding works [37]. Conformational searches of selected compounds were performed by the Spartan 14 program (Wavefunction, Inc.) in the MMFF force field, with a threshold of 3.0 kJ/mol compared with the minimum energy conformer. The conformers were initially optimized at the b3lyp/6–31g(d,p) in gas. NMR calculations on the optimized conformations and TMS were performed using the means of gauge-independent atomic orbital (GIAO) at the mPW1PW91/6–31g(d,p) level, and the calculated shielding constants were directly submitted to statistical analyses with DP4+ probability by weighing the Boltzmann distribution rate [36,37]. The time-dependent density functional theory (TD-DFT) ECD calculations were conducted in MeCN at the b3lyp/6–31+g(d,p) level for all selected conformers of compounds [37]. Rotatory strengths for a total of 30 excited states were calculated. The ECD spectra were generated using SpecDis version 1.6 (University of Würzburg, Würzburg) from dipole-length rotational strengths by applying Gaussian band shapes with a σ of 0.3 eV^2 [48].

4.6. In vitro antibacterial susceptibility assays

The minimum inhibitory concentration (MIC) was evaluated by 96-well micro-dilution method based on previous reports [31,49]. In brief, overnight cultures of the bacteria were suspended into the Cation-adjusted Mueller-Hinton II broth (CAMHB) reaching a bacterial suspension of 0.5 McFarland turbidity [$(1 \sim 2) \times 10^8$ CFU/mL)]. Compounds were dissolved with DMSO to 2.0 mg/mL as stock solutions. All the samples were diluted with CAMHB to 64 μg/mL as the initial concentration. Further two-fold serial dilutions were performed to make their final concentrations in 96-well plates ranging from 64 μg/mL to 0.125 μg/mL. 100 μL of bacterial dilution (5×10^5 CFU/mL) was distributed in each well, as well as negative controls, growth controls (containing culture broth with equal amounts of DMSO, without compounds) and positive controls [containing culture broth plus vancomycin hydrochloride (Van. HCl)]. The 96-well plates were incubated at 37 °C for 16 h and the MIC values of the tested compounds were defined as the lowest concentration to completely inhibit bacterial growth. All the tests were performed in triplicate.

4.7. Statistical analysis

The data were analyzed for their variances by one-way ANOVA using Graphpad prism (version 9). Differences were assessed by Tukey's multiple comparison statistical analysis and determined to be significant at $p < 0.05$.

4.8. Molecular docking study

The ligand structures were optimized using the MM2 energy-minimized function in the Chem3D Ultra version 16.0. The crystal structures of the receptor proteins (Table S8) were obtained from Protein Data Bank [50,51]. AutoDockTools version 1.5.6 were used to prepare the receptor proteins and ligands for the molecular docking experiment. AutoDock Vina programme was used to perform the docking and calculate the binding affinity [52,53]. And lastly, the results were processed and analysed using the BIOVIA, Dassault Systèmes, Discovery Studio Visualizer, v21.1.0.20298, San Diego: Dassault Systèmes, 2023.

Supplementary Material

Refer to Web version on PubMed Central for supplementary material.

Acknowledgements

This work was supported by grants from the National Natural Science Foundation of China (Nos. 21937002, 81773599, 82003659) and NCCIH RO1AT0072318–01 (MTH).

References

[1]. Rudd KE, Johnson SC, Agesa KM, Shackelford KA, Tsoi D, Kievlan DR, Colombara DV, Ikuta KS, Kissoon N, Finfer S, Fleischmann-Struzek C, Machado FR, Reinhart KK, Rowan K, Seymour CW, Watson RS, West TE, Marinho F, Hay SI, Lozano R, Lopez AD, Angus DC, Murray CJL, Naghavi M, Global, regional, and national sepsis incidence and mortality, 1990–2017: analysis for the global burden of disease study, Lancet 395 (2020) 200–211. [PubMed: 31954465]

[2]. Polat G, Ugan RA, Cadirci E, Halici Z, Sepsis and septic shock: current treatment strategies and new approaches, Eurasian, J. Med. 49 (2017) 53–58. [PubMed: 28416934]

[3]. Ahmad-Mansour N, Loubet P, Pouget C, Dunyach-Remy C, Sotto A, Lavigne J-P, Molle V, Staphylococcus aureus toxins: an update on their pathogenic properties and potential treatments, Toxins 13 (2021) 677. [PubMed: 34678970]

[4]. Nishimura NY, Kewcharoen J, Narimasu T, Extremely elevated procalcitonin in a case of acetaminophen overdose and acute liver injury, Intern. Med. 61 (2022) 115–118. [PubMed: 34176834]

[5]. Deresinski S, Counterpoint: vancomycin and *Staphylococcus aureus*—an antibiotic enters obsolescence, Clin. Infect. Dis. 44 (2007) 1543–1548. [PubMed: 17516396]

[6]. Ivanovic I, Boss R, Romanò A, Guédon E, Le-Loir Y, Luini M, Graber HU, Penicillin resistance in bovine *Staphylococcus aureus*: genomic evaluation of the discrepancy between phenotypic and molecular test methods, J. Dairy Sci. 106 (2023) 462–475. [PubMed: 36424317]

[7]. Rossiter SE, Fletcher MH, Wuest WM, Natural products as platforms to overcome antibiotic resistance, Chem. Rev. 117 (2017) 12415–12474. [PubMed: 28953368]

[8]. Newman DJ, Cragg GM, Natural products as sources of new drugs over the nearly four decades from 01/1981 to 09/2019, J. Nat. Prod. 83 (2020) 770–803. [PubMed: 32162523]

[9]. Iskandar K, Murugaiyan J, Hammoudi Halat D, Hage SE, Chibabhai V, Adukkadukkam S, Roques C, Molinier L, Salameh P, Van Dongen M, Antibiotic discovery and resistance: the chase and the race, Antibiotics 11 (2022) 182. [PubMed: 35203785]

[10]. Xiong J, Zhou P-J, Jiang H-W, Huang T, He Y-H, Zhao Z-Y, Zang Y, Choo Y-M, Wang XJ, Chittiboyina AG, Pandey P, Hamann MT, Li J, Hu J-F, Forrestiacids A and B, Pentaterpene inhibitors of ACL and lipogenesis: extending the limits of computational NMR methods in the structure assignment of complex natural products, Angew. Chem. Int. Ed. 60 (2021) 22270–22275.

[11]. Zhou P-J, Huang T, Ma G-L, Tong Y-P, Chen W-X, Zang Y, Xiong J, Li J, Hu J-F, Forrestiacids C and D, unprecedented triterpene-diterpene adducts from *Pseudotsuga forrestii*, J. Nat. Prod. 86 (2022) 1251–1260.

[12]. Zou YK, Wang XJ, Sims J, Wang B, Pandey P, Welsh CL, Stone RP, Avery MA, Doerksen RJ, Ferreira D, Anklin C, Valeriote FA, Kelly M, Hamann MT, Computationally assisted discovery and assignment of a highly strained and PANC-1 selective alkaloid from Alaska's deep ocean, J. Am. Chem. Soc. 141 (2019) 4338–4344. [PubMed: 30758203]

[13]. Ibrahim MA, Mansoor AA, Gross A, Ashfaq MK, Jacob M, Khan SI, Hamann MT, Methicillin-resistant Staphylococcus aureus (MRSA)-active metabolites from Platanus occidentalis (american sycamore), J. Nat. Prod. 72 (2009) 2141–2144. [PubMed: 19904995]

[14]. Ribeiro J, Silva V, Aires A, Carvalho R, Barros L, Gaivão I, Igrejas G, Poeta P, Platanus hybrida's phenolic profile, antioxidant power, and antibacterial activity against methicillin-resistant Staphylococcus aureus (MRSA), Horticulturae 8 (2022) 243.

[15]. Schrader KK, Hamann MT, McChesney JD, Rodenburg DL, Ibrahim MA, Antibacterial activities of metabolites from Platanus occidentalis (american sycamore) against fish pathogenic bacteria, J. Aquac. Res. Dev. 6 (2015) 364. [PubMed: 27790379]

[16]. Shaw JJ, Swartz K, Valeriote F, Media J, Chen B, Hamann MT, Wang XJ, Identification of the metabolites of a novel anti-MRSA compound, kaempferol-3-O-alpha-L-(2“,3”-di-p-coumaroyl)rhamnoside (KCR), extracted from american sycamore, Nat. Prod. Commun. 13 (2018) 355–358.

[17]. Zhang YG, Valeriote F, Swartz K, Chen B, Hamann MT, Rodenburg DL, McChesney JD, Shaw JJ, HPLC plasma assay of a novel anti-MRSA compound, kaempferol-3-O-alpha-L-(2“,3”-di-p-coumaroyl)rhamnoside, from sycamore leaves, Nat. Prod. Commun. 10 (2015) 1383–1386. [PubMed: 26434123]

[18]. Tantry MA, Akbar S, Dar JA, Irtiza S, Galal A, Khuroo MA, Ghazanfar K, Acylated flavonol glycoside from Platanus orientalis, Fitoterapia 83 (2012) 281–285. [PubMed: 22119764]

[19]. Mitrokotsa D, Mitaku S, Demetzos C, Harvala C, Mentis A, Perez S, Kokkinopoulos D, Bioactive compounds from the buds of *Platanus orientalis* and isolation of a new kaempferol glycoside, Planta Med. 59 (1993) 517–520. [PubMed: 8302950]

[20]. Barron D, Aidi CE, Mariotte A-M, ^{13}C nuclear magnetic resonance analysis of two prenyl flavonols from *Platanus acerifolia* buds, Phytochem. Anal. 5 (1994) 309–314.

[21]. Kaouadji M, Further prenylated flavonols from *Platanus acerifolia*'s unripe buds, Tetrahedron Lett. 55 (2014) 1285–1288.

[22]. Kaouadji M, Morand JM, Gilly C, 4-Hydroxygrenoblone, another uncommon C-prenylated flavonoid from *Platanus acerifolia* buds, J. Nat. Prod. 49 (1986) 508–510.

[23]. Kaouadji M, Ravanel P, Mariotte A-M, New prenylated flavonols from *Platanus acerifolia* buds, J. Nat. Prod. 49 (1986) 153–155.

[24]. Kaouadji M, Ravanel P, Tissut M, Creuzet S, Novel methylated flavonols with unsubstituted B ring from *Platanus acerifolia* buds, J. Nat. Prod. 51 (1988) 353–356.

[25]. Kaouadji M, Morand J-M, Garcia J, Further acylated kaempferol rhamnosides from *Platanus acerifolia* buds, J. Nat. Prod. 56 (1993) 1618–1621.

[26]. Kaouadji M, Champavier Y, Morand J-M, *Platanus acerifolia*'s buds: additional non-polar metabolites and structure revision of two previous dihydrochalcone-like metabolites, Tetrahedron Lett. 54 (2013) 6352–6357.

[27]. Thai QD, Tchoumtchoua J, Makropoulou M, Boulaka A, Meligova AK, Mitsiou DJ, Mitakou S, Michel S, Halabalaki M, Alexis MN, Skaltsounis LA, Phytochemical study and biological evaluation of chemical constituents of *Platanus orientalis* and *Platanus×acerifolia* buds, Phytochemistry 130 (2016) 170–181. [PubMed: 27179684]

[28]. Zuo B, Liao Z-X, Xu C, Liu C, Two novel prenylated kaempferol derivatives from fresh bud's fur of Platanus acerifolia and their anti-proliferative activities, Nat. Prod. Res. 30 (2016) 2523–2528. [PubMed: 26736086]

[29]. Chen H-F, Huang R-Z, Zuo B, Ji L-J, Mo Z-J, Liao Z-X, Anti-proliferative activities of two flavonols with unsubstituted B-ring from the leaves of Platanus acerifolia, Nat. Prod. Commun. 12 (2017) 1701–1704.

[30]. Liu QY, Song ZJ, Han H, Donkor S, Jiang LH, Wang WY, Chu HQ, A novel green reinforcement corrosion inhibitor extracted from waste Platanus acerifolia leaves, Constr. Build. Mater. 260 (2020) 119695.

[31]. Wu XY, Tang Y, Osman EEA, Wan J, Jiang W, Yang G-X, Xiong J, Zhu QG, Hu J-F, Bioassay-guided isolation of new flavonoid glycosides from Platanus×acerifolia leaves and their Staphylococcus aureus inhibitory effects, Molecules 27 (2022) 5357. [PubMed: 36080125]

[32]. Flores SE, Herrán J, The structure of pendulin and penduletin: a new flavonol glucoside isolated from *brickelia pendula*, Tetrahedron 2 (1958) 308–315.

[33]. Tu FJ, Dai Y, Yao ZH, Wang XL, Yao XS, Qin L, Flavonol glycosides from *Epimedium pubescens*, Chem. Pharm. Bull. 59 (2011) 1317–1321.

[34]. Ma G-L, Xiong J, Yang G-X, Pan L-L, Hu C-L, Wang W, Fan H, Zhao Q-H, Zhang H-Y, Hu J-F, Biginkgosides A−I, unexpected minor dimeric flavonol diglycosidic truxinate and truxillate esters from *Ginkgo biloba* leaves and their antineuroinflammatory and neuroprotective activities, J. Nat. Prod. 79 (2016) 1354–1364. [PubMed: 27140807]

[35]. Ho J-C, Chen C-M, Row L-C, Flavonoids and benzene derivatives from the flowers and fruit of tetrapanax papyriferus, J. Nat. Prod. 68 (2005) 1773–1775. [PubMed: 16378372]

[36]. Grimblat N, Zanardi MM, Sarotti AM, Beyond DP4: an improved probability for the stereochemical assignment of isomeric compounds using quantum chemical calculations of NMR shifts, J. Org. Chem. 80 (2015) 12526–12534. [PubMed: 26580165]

[37]. Liang K-Y, Li H, Zhou P-J, Zhao Z-Y, Zang Y, Xiong J, Li J, Hu J-F, Squamabietenols A-F, undescribed abietane-O-abietane dimeric diterpenoids from the ornamental conifer Juniperus squamata and their ATP-citrate lyase inhibitory activities, Phytochemistry 210 (2023) 113663. [PubMed: 36990194]

[38]. Yahagi T, Daikonya A, Kitanaka S, Flavonol acylglycosides from flower of *Albizia julibrissin* and their inhibitory effects on lipid accumulation in 3T3-L1 Cells, Chem. Pharm. Bull. 60 (2012) 129–136.

[39]. Cheng X-X, Guo C-C, Yang Q, Tang X-M, Zhang C-R, Isolation and identification of radical scavenging components of seeds of *Desmodium styracifolium*, Chem. Nat. Compd. 53 (2017) 36–39.

[40]. Macheboeuf P, Contreras-Martel C, Job V, Dideberg O, Dessen A, Penicillin binding proteins: key players in bacterial cell cycle and drug resistance processes, FEMS Microbiol. Rev. 30 (2006) 673–691. [PubMed: 16911039]

[41]. Moir DT, Identification of inhibitors of bacterial enoyl-acyl carrier protein reductase, Curr. Drug Targets - Infect. Disord. 5 (2005) 297–305. [PubMed: 16181147]

[42]. Lu H, Tonge PJ, Inhibitors of FabI, an enzyme drug target in the bacterial fatty acid biosynthesis pathway, Acc. Chem. Res. 41 (2008) 11–20. [PubMed: 18193820]

[43]. Sauvage E, Kerff F, Terrak M, Ayala JA, Charlier P, The penicillin-binding proteins: structure and role in peptidoglycan biosynthesis, FEMS Microbiol. Rev. 32 (2008) 234–258. [PubMed: 18266856]

[44]. Zapun A, Contreras-Martel C, Vernet T, Penicillin-binding proteins and β-lactam resistance, FEMS Microbiol. Rev. 32 (2008) 361–385. [PubMed: 18248419]

[45]. Diao XT, Ye F, Zhang MN, Ren XT, Tian XX, Lu JP, Sun XN, Hou Z, Chen XY, Li FW, Zhuang JJ, Ding H, Peng C, Rastinejad F, Luo C, Wu DL, Identification of oleoylethanolamide as an endogenous ligand for HIF-3α, Nat. Commun. 13 (2022) 2529. [PubMed: 35534502]

[46]. Lu GW, Hu YW, Wang QH, Qi JX, Gao F, Li Y, Zhang YF, Zhang W, Yuan Y, Bao JK, Zhang BC, Shi Y, Yan JH, Gao GF, Molecular basis of binding between novel human coronavirus MERS-CoV and its receptor CD26, Nature 500 (2013) 227–231. [PubMed: 23831647]

[47]. Xiong H, Han J, Wang J, Lu WC, Wang C, Chen Y, Lian FL, Zhang NX, Liu Y-C, Zhang CH, Ding H, Jiang HL, Lu WC, Luo C, Zhou B, Discovery of 1,8-acridinedione derivatives as novel GCN5 inhibitors via high throughput screening, Eur. J. Med. Chem. 151 (2018) 740–751. [PubMed: 29665527]

[48]. Bruhn T, Schaumloffel A, Hemberger Y, Bringmann G, SpecDis: quantifying the comparison of calculated and experimental electronic circular dichroism spectra, Chirality 25 (2013) 243–249. [PubMed: 23532998]

[49]. Chen B, Qiu PJ, Xu BF, Zhao QM, Gu Y-C, Fu L, Bi SJ, Lan LF, Wang C-Y, Guo Y-W, Cytotoxic and antibacterial isomalabaricane terpenoids from the sponge Rhabdastrella globostellata, J. Nat. Prod. 85 (2022) 1799–1807. [PubMed: 35767002]

[50]. Berman HM, Westbrook J, Feng Z, Gilliland G, Bhat TN, Weissig H, Shindyalov IN, Bourne PE, The protein data bank, Nucleic Acids Res. 28 (2000) 235–242. [PubMed: 10592235]

[51]. Burley SK, Berman HM, Bhikadiya C, Bi C, Chen L, Di Costanzo L, Christie C, Dalenberg K, Duarte JM, Dutta S, Feng Z, Ghosh S, Goodsell DS, Green RK, Guranovic V, Guzenko D, Hudson BP, Kalro T, Liang YH, Lowe R, Namkoong H, Peisach E, Periskova I, Prlic A, Randle C, Rose A, Rose P, Sala R, Sekharan M, Shao CH, Tan LH, Tao Y-P, Valasatava Y, Voigt M, Westbrook J, Woo J, Yang H, Young J, Zhuravleva M, Zardecki C, RCSB protein data bank:

biological macromolecular structures enabling research and education in fundamental biology, biomedicine, biotechnology and energy, Nucleic Acids Res. 47 (2019) D464–D474. [PubMed: 30357411]

[52]. Sanner MF, Python: a programming language for software integration and development, J. Mol. Graphics Modell. 17 (1998) 57–61.

[53]. Trott O, Olson AJ, AutoDock Vina: improving the speed and accuracy of docking with a new scoring function, efficient optimization, and multithreading, J. Comput. Chem. 31 (2010) 455–461. [PubMed: 19499576]

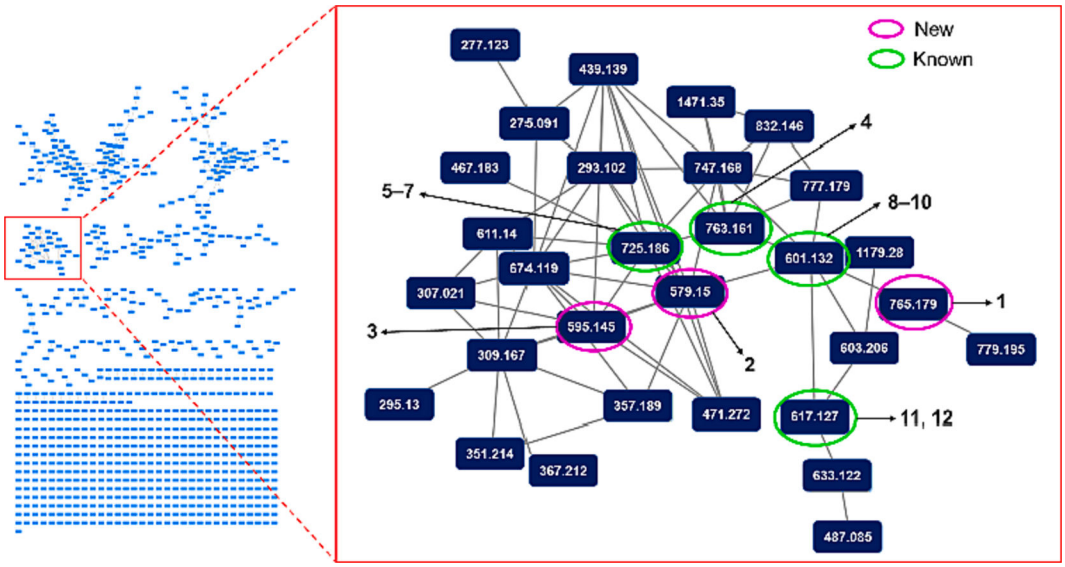

Fig. 1.

MoIN of the mentioned bioactive fraction. left: Organized landscape of complete network; right: the MoIN cluster with signals at *m*/*z* 579, 595, and 765 for new PTSs and at *m*/*z* 763, 725, 617, and 601 for known PTSs.

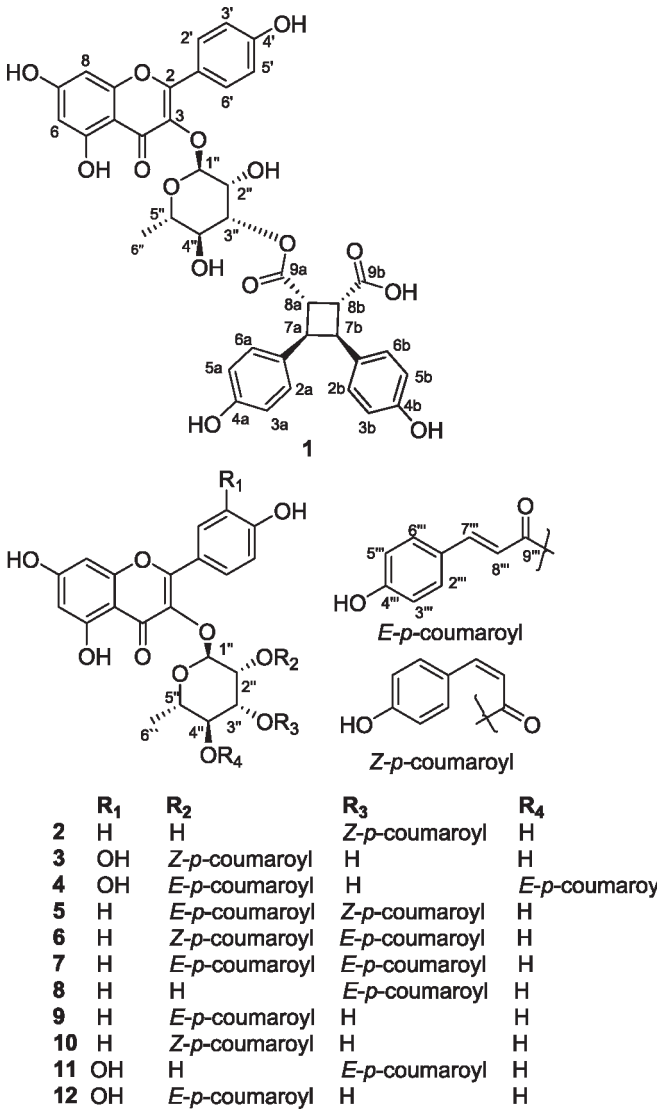

	R_1	R_2	R_3	R_4
2	H	H	*Z*-*p*-coumaroyl	H
3	OH	*Z*-*p*-coumaroyl	H	H
4	OH	*E*-*p*-coumaroyl	H	*E*-*p*-coumaroy
5	H	*E*-*p*-coumaroyl	*Z*-*p*-coumaroyl	H
6	H	*Z*-*p*-coumaroyl	*E*-*p*-coumaroyl	H
7	H	*E*-*p*-coumaroyl	*E*-*p*-coumaroyl	H
8	H	H	*E*-*p*-coumaroyl	H
9	H	*E*-*p*-coumaroyl	H	H
10	H	*Z*-*p*-coumaroyl	H	H
11	OH	H	*E*-*p*-coumaroyl	H
12	OH	*E*-*p*-coumaroyl	H	H

Fig. 2.
The structures of compounds of **1**–**12**.

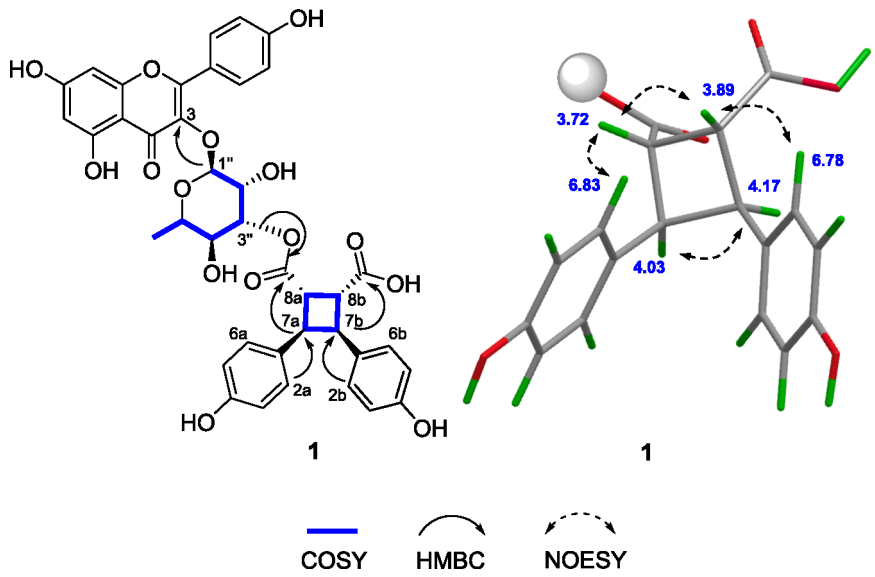

Fig. 3.
Key 2D-NMR correlations of compound **1**.

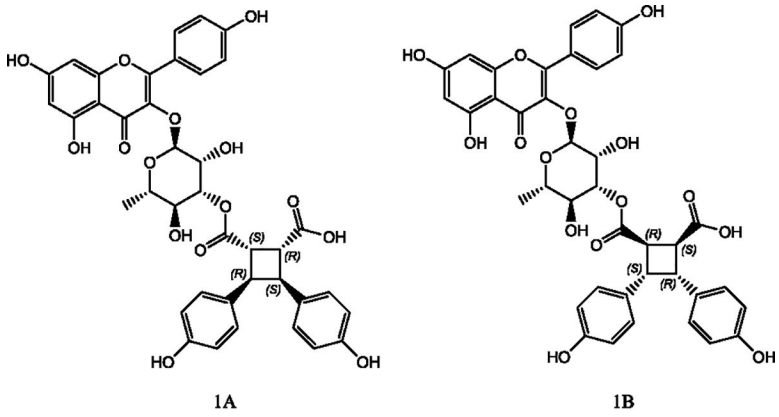

	1A	1B
sDP4+ (H data)	–	–
sDP4+ (C data)	99.83%	0.17%
sDP4+ (all data)	99.83%	0.17%
uDP4+ (H data)	–	–
uDP4+ (C data)	97.68%	2.32%
uDP4+ (all data)	97.68%	2.32%
DP4+ (H data)	–	–
DP4+ (C data)	100.00%	0.00%
DP4+ (all data)	100.00%	0.00%

Fig. 4.

NMR calculations and DP4+ analysis outcomes of stereoisomers **1**A and **1**B using the means of GIAO at mPW1PW91/6–31g (d, p) level.

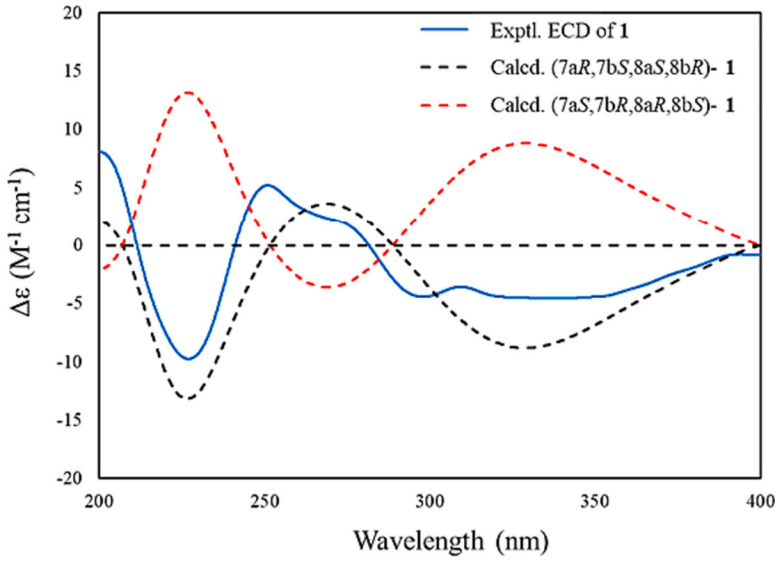

Fig. 5.
Experimental and calculated ECD spectra of **1** in MeCN.

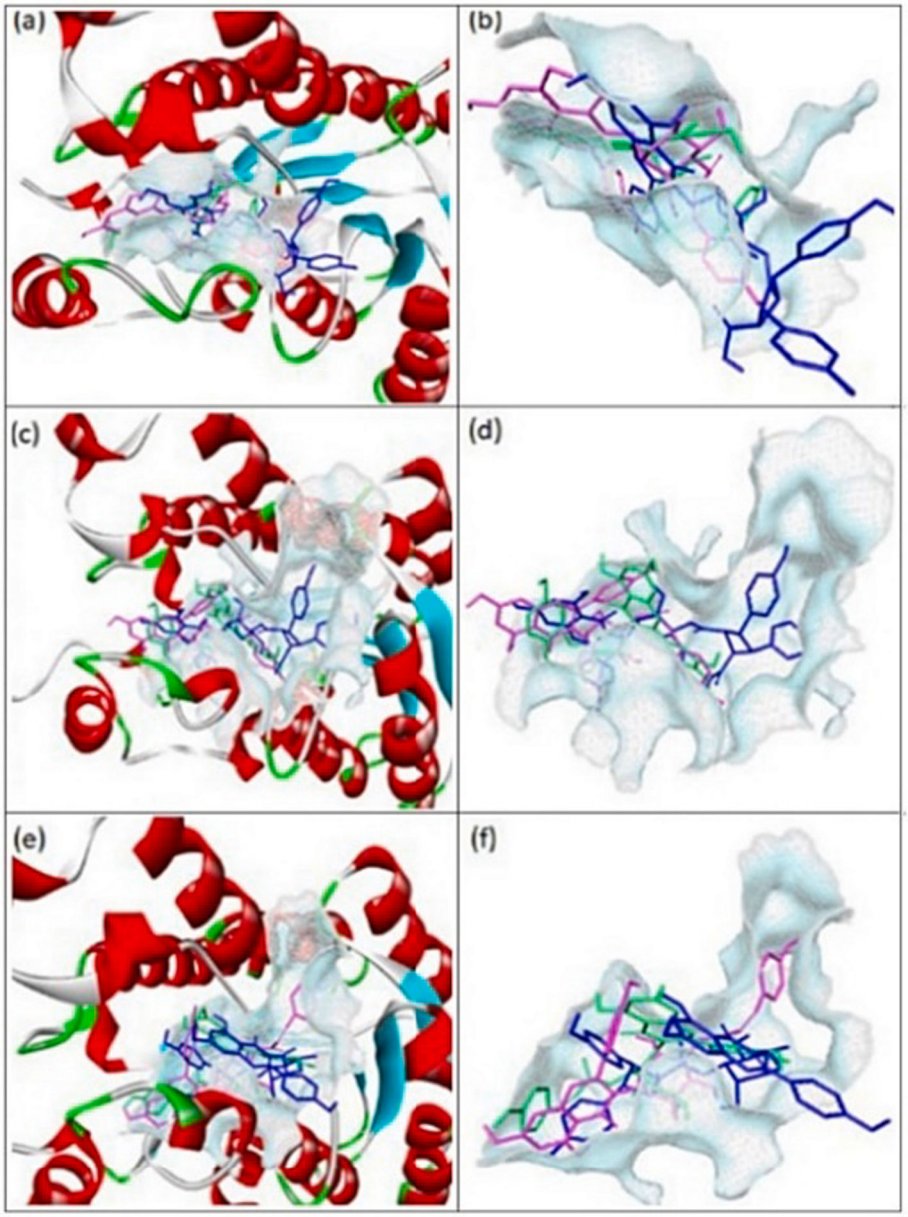

Fig. 6.

The binding of compounds **1** (blue), **2** (pink), and **3** (green) to (a) *S. aureus* FabI; (b) binding domain of *S. aureus* FabI; (c) *A. baumannii* FabI; (d) binding domain of *A. baumannii* FabI; (e) *P. aeruginosa* FabI; (f) binding domain of *P. aeruginosa* FabI.

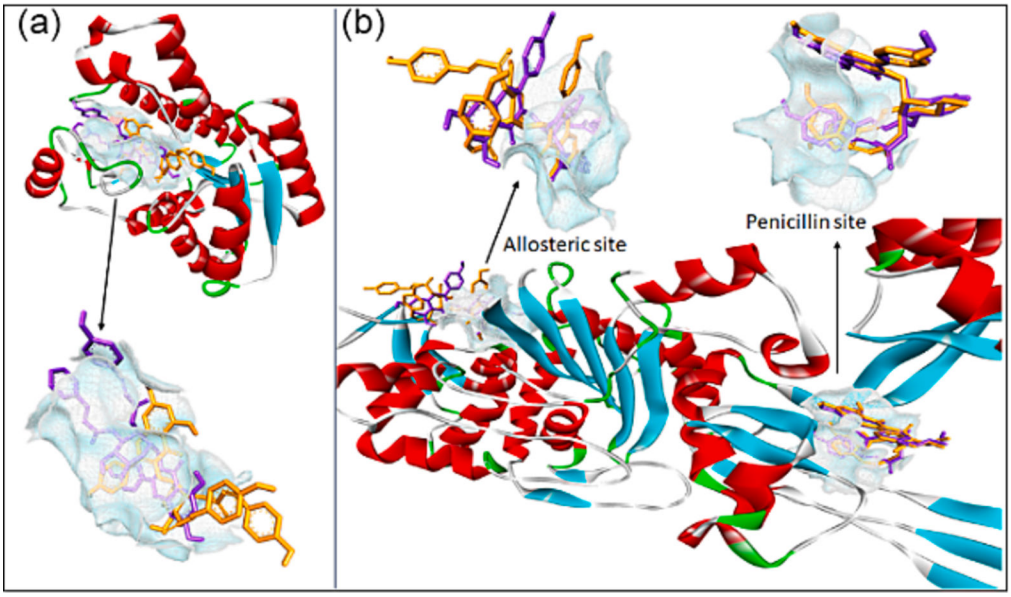

Fig. 7.

The binding of compounds **6** (orange) and **7** (purple) to (a) *S. aureus* FabI and (b) *S. aureus* PBP2.

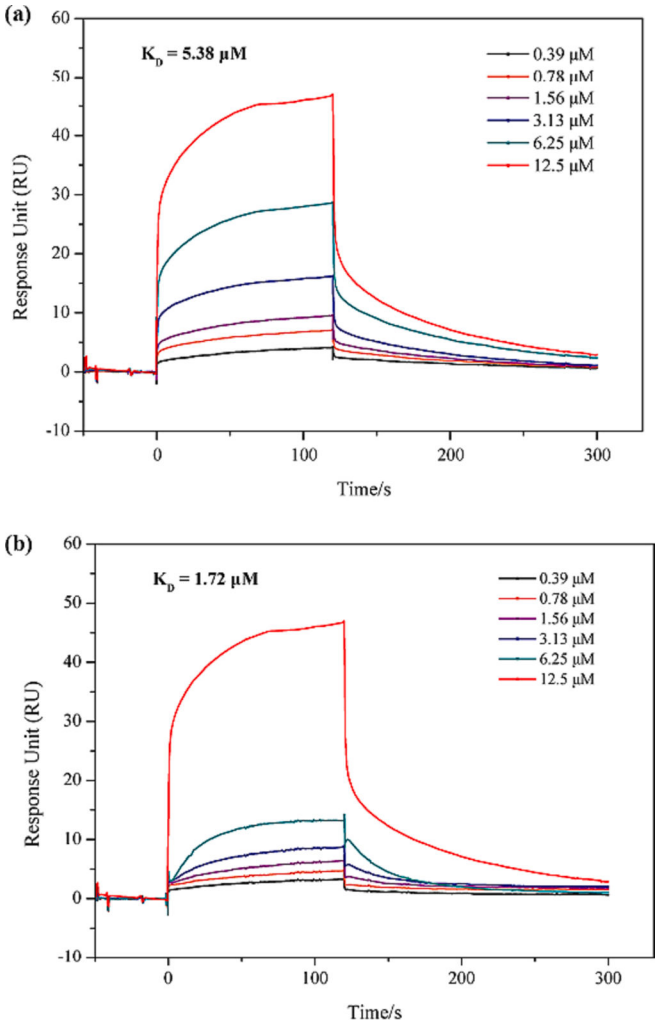

Fig. 8.

SPR-based binding assay of **1** (a) and **7** (b) with FabI. The compounds were prepared at concentrations of 0.39 μM, 0.78 μM, 1.56 μM, 3.13 μM, 6.25 μM, and 12.5 μM, respectively. K_D is the equilibrium dissociation constant, a basic parameter to evaluate the binding property of the compound-receptor.

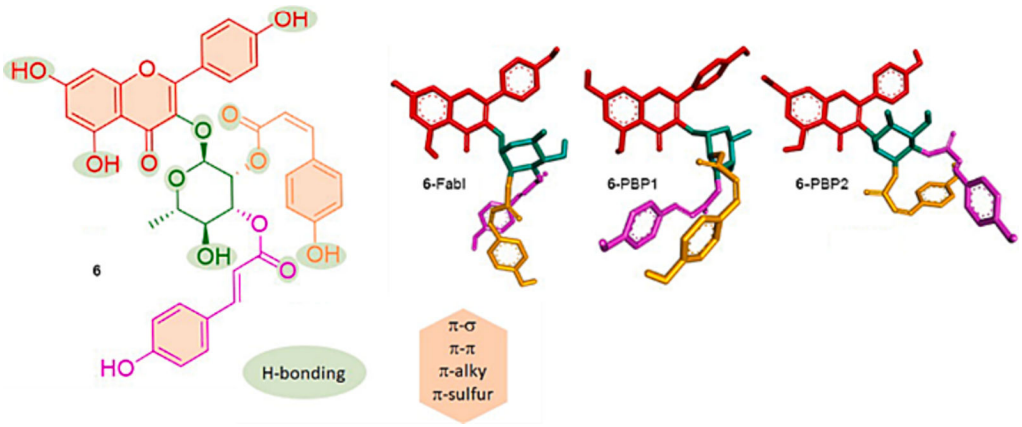

Fig. 9.

Binding poses and interactions of **6** to FabI, PBP1, and PBP2.

Table 1

In vitro antibacterial activity of the isolated PTSs.

Compound	MIC (μg/mL)	
	Mu50	Van (B)
6	4^{c}	0.5^{c}
7	16^{a}	1^{b}
Van. HCl	8^{b}	256^{a}

Mu50: methicillin-resistant *S. aureus*; Van (B): glycopeptide-resistant *E. faecium*. Different superscript letters (i.e., a-c) indicate significant differences among the compounds in each column at $p < 0.05$.